THE JOURNAL OF BIOLOGICAL CHEMISTRY VOL. 290, NO. 29, pp. 17848–17862, July 17, 2015

Ctr9, a Protein in the Transcription Complex Paf1, Regulates Dopamine Transporter Activity at the Plasma Membrane*

Received for publication, February 19, 2015, and in revised form, May 27, 2015 Published, JBC Papers in Press, June 5, 2015, DOI 10.1074/jbc.M115.646315

Stéphanie De Gois[‡§¶‖], Patrick Slama[‡§¶1], Nicolas Pietrancosta[‡‡1], Amaia M. Erdozain[‡§¶], Franck Louis[‡§¶], Caroline Bouvrais-Veret[‡§¶], Laurent Daviet[§§], and Bruno Giros[‡§¶‖2]**

From the [‡]INSERM U952 and [§]CNRS UMR 7224, 75005 Paris, France, [¶]Université Pierre et Marie Curie, Neuroscience Paris Seine, 75005 Paris, France, [‖]Douglas Hospital Research Center, Department of Psychiatry, McGill University, Montreal H4H 1R3 Quebec, Canada, [**]Université Paris Descartes, Sorbonne Paris Cité, [‡‡]CNRS, UMR 8601, 75006 Paris, France, and [§§]Hybrigenics, 3–5 Impasse Reille, 75014 Paris, France

Background: The dopamine transporter controls the concentration of dopamine at the synapse.
Results: Ctr9, formerly identified as a nuclei protein, interacts with the dopamine transporter in the cytoplasmic compartment.
Conclusion: This interaction facilitates the targeting of the dopamine transporter to the plasma membrane and increases its activity.
Significance: Identifying the complete dopamine transporter interactome is essential to understanding how neurotransmission is regulated.

Dopamine (DA) is a major regulator of sensorimotor and cognitive functions. The DA transporter (DAT) is the key protein that regulates the spatial and temporal activity of DA release into the synaptic cleft via the rapid reuptake of DA into presynaptic termini. Several lines of evidence have suggested that transporter-interacting proteins may play a role in DAT function and regulation. Here, we identified the tetratricopeptide repeat domain-containing protein Ctr9 as a novel DAT binding partner using a yeast two-hybrid system. We showed that Ctr9 is expressed in dopaminergic neurons and forms a stable complex with DAT *in vivo* via GST pulldown and co-immunoprecipitation assays. In mammalian cells co-expressing both proteins, Ctr9 partially colocalizes with DAT at the plasma membrane. This interaction between DAT and Ctr9 results in a dramatic enhancement of DAT-mediated DA uptake due to an increased number of DAT transporters at the plasma membrane. We determined that the binding of Ctr9 to DAT requires residues YKF in the first half of the DAT C terminus. In addition, we characterized Ctr9, providing new insight into this protein. Using three-dimensional modeling, we identified three novel tetratricopeptide repeat domains in the Ctr9 sequence, and based on deletion mutation experiments, we demonstrated the role of the SH2 domain of Ctr9 in nuclear localization. Our results demonstrate that Ctr9 localization is not restricted to the nucleus, as previously described for the transcription complex Paf1. Taken together, our data provide evidence that Ctr9 modulates DAT function by regulating its trafficking.

The importance of dopamine (DA)[3]-mediated neurotransmission is emphasized by its direct implication in neurological and psychiatric disorders, such as Parkinson disease, dystonia, schizophrenia, attention deficit/hyperactivity disorder, Tourette syndrome, and drug addiction (1). These disorders share DA transmission dysfunction as a common pathological mechanism. The key to understanding and reversing the pathophysiology of these disorders as well as understanding the normal functioning of DA synapses and systems is to develop a comprehensive profile of the various processes that are involved in establishing synaptic DA flux (2, 3).

The DA transporter (DAT) is the key protein that removes DA from the synaptic cleft via an ionic gradient-dependent reuptake mechanism (4). By draining DA from the extracellular space in only a few hundred milliseconds, DAT regulates the availability of DA, which activates pre- and post-synaptic DA receptors, in both time and space. The importance of this reuptake process is sustained by the profound consequences of its blockade using psychostimulant drugs (such as amphetamine, cocaine, and methylphenidate) or genetic loss of function (5). Indeed, DAT genetic deletion in mice results in severe behavioral and neurochemical changes, including hyperlocomotor activity, increased DA receptor responsiveness, and sensitization to psychostimulants (5–7).

Previous studies have shown that DAT activity can be altered via regulation by protein kinases (for review, see Ref. 8). This regulatory activity appears to involve the rapid translocation of DAT from the cell membrane (9–11). Nevertheless, the mechanisms underlying this regulatory activity are poorly understood. For instance, it has been demonstrated that PKC activation leads to DAT internalization, but when all DAT phosphorylation sites are mutated, its removal from the cell surface

* This work was supported by Canadian Institutes for Health Research Operating Grant 240843 and by INSERM/CNRS/Université Pierre et Marie Curie funding (to B. G.). Post doctoral support was provided by grants from the Fondation pour la Recherche Médicale and the Basque Government (to A. M. E.), "Schizo'Oui" association, and the Canadian Institutes for Health Research. The authors declare that they have no conflicts of interest with the contents of this article.

[1] Both authors contributed equally to this work.

[2] To whom correspondence should be addressed: Douglas Hospital Research Center, Department of Psychiatry, McGill University, Montreal H4H 1R3 Quebec, Canada. Tel.: 514-261-0520; Fax: 514-762-3034; E-mail: bruno.giros@mcgill.ca or bruno.giros@upmc.fr.

[3] The abbreviations used are: DA, dopamine; DAT, DA transporter; hDAT, human DAT; CT, C terminus; TPR, tetratricopeptide repeat; TPRD, TPR domain; DS, Discovery Studio; Bis-Tris, 2-[bis(2-hydroxyethyl)amino]-2-(hydroxymethyl)propane-1,3-diol; SH2, Src homology-2; NET, norepinephrine transporter; VTA, ventral tegmental area; shScr, scrambled shRNA; shm, shRNA against mouse Ctr9; ER, endoplasmic reticulum.

is not prevented (12, 13). Several DAT binding partners have been suggested to be involved in the modulation of DAT stability, localization, trafficking, and/or activity. A study by Lee *et al.* (14) showed that DAT activity is affected by a direct interaction between the C terminus of DAT (DAT-CT) and α-synuclein. DAT function is also regulated by its interaction with the PDZ-containing-domain PKC-interacting protein-1 (PICK1; Ref. 15), the focal adhesion protein HIC-5 (16), receptor for activated C-kinase1 (RACK1), the SNARE component syntaxin-1A (17), parkin (18), the DA receptors D_2 and D_3 (19, 20), synaptogyrin-3 (21), the GTPase Rin (22), and the G protein βγ subunits (23).

To discover new DAT-associated proteins, we performed a yeast two-hybrid screen using the DAT-CT, and we identified the tetratricopeptide repeat (TPR) domain (TPRD)-containing protein Ctr9 (24) as a strong DAT-interacting protein. Ctr9 was previously identified as a member of the transcription complex Paf1, with multiple functions in transcription-related activities (25, 26). Thus, Ctr9 represents a novel example of a protein that performs dual nuclear and cytoplasmic functions.

Experimental Procedures

Yeast Two-hybrid Screening—Yeast two-hybrid screening was performed on a rat brain cDNA library using the intracellular DAT-CT (Hybrigenics, Paris, France) as bait as previously described (27). Polymerase chain reaction (PCR) was performed to generate a DAT-GAL4 DNA binding domain fusion construct containing the rat DAT-CT (Tyr^{574}-Leu^{619}) in the pB6 vector (Hybrigenics).

For complementation experiments in yeast, the bait and prey plasmids were generated by subcloning PCR fragments of the DAT-CT and Ctr9 sequences, respectively, in the pB6 (bait) and pP6 (prey) vectors (Hybrigenics). The bait and prey constructs were transformed into the yeast strains CG1945 and YHGX13, respectively, using the lithium acetate method, and these strains were cultured at 30 °C for 3–5 days on yeast extract/peptone/dextrose plates lacking tryptophan (bait) or leucine (prey). Yeast mating was performed via overnight incubation of both yeast strains in 0.5 ml of extract/peptone/dextrose medium with shaking. The resulting mixture was then spotted on plates containing leucine- and tryptophan-deficient medium and was cultured for 3–5 days at 30 °C. Specific interactions between the bait and prey constructs were verified either by the growth of yeast colonies in leucine-, tryptophan-, and histidine-free medium after 3–5 days at 30 °C or by a β-galactosidase assay.

Mutagenesis and Construction of the DAT and Ctr9 Mutants—All of the deletion mutants were constructed via PCR using primers beginning at the 5′- or 3′-end of the desired sequence. For DAT point mutations, we used the QuikChange site-directed mutagenesis kit (Stratagene) and a set of complementary primers. All clones were sequenced in both directions before use. The plasmids were purified using a Plasmid Maxi Kit (Qiagen) before use.

Protein Sequence Analysis—We selected DAT-CT and the TPRDs of CTR9 (specifically the region from the final seven amino acids of TPRD6 to the first eight residues of TPRD10). All sequences were obtained from the ExPASy molecular biology server 32. Multiple sequence alignment was performed utilizing both the PSI-blast algorithm in the NCBI server and the multiple sequence alignment protocol in Discovery Studio (DS) software. The scoring function used was Blosum62 in the case of the DS protocol (28, 29). Blasts searches were performed against the PDB database to identify similar structures. The different results were compared and manually analyzed.

Secondary Structure Prediction—Secondary structure predictions of the entire structures were performed using the free software TMHMM (30) and HMMTOP (31), and only two templates (PDB entries 1VFH and 2NQS), and the partially crystallized DAT-CT (PDB entry 4M48) appeared to be partially relevant.

Homology Models Generation—A sequence alignment of Ctr9 and DAT-CT domains with crystallized proteins was generated according to Malherbe *et al.* (32) and was further refined using predicted and known secondary structures. Homology models for DAT-CT and the TPRDs of CTR9 were generated using the automated comparative modeling tool MODELER 9.0 (DS Modeling 2.5; Accelrys; Ref. 33) as previously described (34, 35). Models were generated using the coordinates of a mutant of the molybdopterin biosynthesis protein MoeA (PDB code 2NQS), DAT itself (PDB code 4M48), and alanine racemase (PDB code 1VFH) as templates for DAT-CT and the superhelical TPRD of *O*-linked GlcNAc transferase (PDB code 1W3B) as a template for CTR9. The structural quality of the models was assessed according to the MODELER probability density functions and Profiles-3D analysis (DS Modeling 2.5) and was confirmed by the Ramachandran diagram (Fig. 3*D*; Ref. 36). The loops were refined using MODELER. The final model was used for docking experiments.

Protein-Protein Docking—The protein-protein docking experiment was performed using the protein docking (ZDOCK) module (DS Modeling 2.5; Ref. 35). Docking was performed without any constraints or specific residue selection for the Ctr9 TPRD and DAT-CT homology models. The obtained poses (2000 per run) were refined using the RDOCK module (DS Modeling 2.5; Ref. 37). All poses were regrouped into several clusters (energy-, number-, and position-based), and the most significant clusters were selected for interaction studies.

Cell Culture and Transfection—Human carcinoid BON cells were obtained from Dr. Gasnier (CNRS UMR8192) and were maintained in 1:1 DMEM/F-12 medium supplemented with 10% fetal bovine serum (PAA Laboratories), 100 units/ml penicillin and 100 μg/ml streptomycin (Life Technologies) at 37 °C in a humidified 5% CO_2 incubator. The BON cells were transiently transfected using Lipofectamine 2000 (Life Technologies) according to the manufacturer's instructions or using a calcium phosphate transfection protocol. Cells were seeded 2 days before transfection on either 12-mm glass coverslips at a density of 1.3×10^5 cells/coverslip (immunocytochemistry), 100-mm Petri dishes at 2.5×10^6 cells/dish (immunoprecipitation and biotinylation experiments), or 24-well plates at 6.5×10^4 cells/well (DA uptake experiments).

Immunoprecipitation—Lysates from transfected BON cells or mouse tissue were prepared in lysis buffer (50 mM Tris-HCl, 150 mM NaCl, 1% Nonidet P-40, and 0.5% sodium deoxycholate). Immunoprecipitations were performed using either

anti-hemagglutinin (HA, Roche Applied Science), anti-DAT (Chemicon), or anti-Ctr9 (Bethyl Laboratories) antibodies. The cleared lysates, 500 μg for cells and 1.5 mg for mouse tissue, were incubated in 10 μg of the appropriate antibody at 4 °C overnight. Protein A-agarose beads (Roche Applied Science) were added, and the samples were incubated for an additional 3 h at 4 °C. The beads were washed 2 times with lysis buffer, 2 times with 50 mM Tris-HCl, 500 mM NaCl, 0.1% Nonidet P-40, and 0.05% sodium deoxycholate and once with 50 mM Tris-HCl, 0.1% Nonidet P-40, and 0.05% sodium deoxycholate. All buffers were supplemented with protease inhibitors. Elution was performed for 30 min at 42 °C followed by 10 min at 70 °C in LDS sample buffer (Life Technologies). The samples were analyzed via Western blotting.

Western Blot Analysis—Protein concentrations were determined via a Bradford assay (Bio-Rad). The proteins were size-fractionated on 10% precast Bis-Tris/MES SDS-polyacrylamide gels (Life Technologies) and were electrophoretically transferred to a nitrocellulose membrane (GE Healthcare) using standard protocols. The membranes were first incubated at room temperature in blocking buffer for 30 min and then incubated overnight at 4 °C in primary antibodies directed against DAT (our rabbit polyclonal antibody, 1:5000, or Chemicon, 1:1000), Ctr9 (Bethyl Laboratories, 1:1000), HA (clone 3F10, Roche Applied Science, 1:3000), or Myc (Clontech, 1:250). After several washes, the bound antibodies were detected using horseradish peroxidase-conjugated anti-rabbit IgG (light chain, Jackson ImmunoResearch) followed by enhanced chemiluminescence and exposure to Hyperfilm ECL (GE Healthcare).

Glutathione S-Transferase (GST) Pulldown Assay—The GST construct was obtained via PCR amplification of the Ctr9 cDNA sequence from residues 298 to 611, fused in-frame to the GST fusion vector PGEX-4T.1 (GE Healthcare), and verified by automated sequencing. The GST-fused plasmid was expressed in BL21 bacterial cells and was isolated using glutathione-agarose beads (GE Healthcare). Then, 50 μg of GST alone or GST-Ctr9 protein coupled to glutathione-agarose beads were incubated in 1 mg of protein lysate from the striatum and the substantia nigra overnight at 4 °C. The mixtures were washed 3 times with 1× PBS containing 0.5% Triton X-100 and protease inhibitors. The protein complexes were eluted in Laemmli buffer, and DAT expression was monitored via Western blotting.

Immunocytochemistry—The cells were processed 48 h after transfection. The culture medium was removed, and the cells were rinsed with 1× PBS and fixed on ice using 4% paraformaldehyde or −20 °C methanol for 10 min. The cells were rinsed 3 times for 10 min with 1× PBS and incubated in blocking buffer (1× PBS, 0.25% Triton X-100, 2% BSA, and 2% normal goat serum) at room temperature for 30 min. A previously characterized polyclonal antibody against rat the N terminus of DAT (38) was diluted 1:1000 in blocking buffer, and the cells were incubated in this antibody overnight at 4 °C. After 3 washes (10 min) with 1× PBS, a species-specific secondary antibody coupled to Alexa 555 (Invitrogen SARL, Cergy-pontoise, France) diluted 1:1000 in blocking buffer was applied for 45 min at room temperature. The nuclei were labeled using DAPI (Sigma, 1:5000). Glass coverslips were mounted on a slide using Fluoromount-G (Clinisciences). Immunolabeling was observed using a ×63 oil-immersion lens (numerical aperture of 1.4) at a 3× digital magnification. All images were acquired via sequential scanning for DAPI, FITC, Cy3, and Cy5 detection using a confocal laser scanning microscope (Leica TCS SP5 microscope equipped with LCS Leica software) or a fluorescence microscope equipped with an Apotome module (Zeiss, Axiovert 200 M).

Double-labeling in Situ Hybridization—RNA transcripts were detected on frozen rat brain sections (14 μm thickness) from adult rats using a fluorescein-conjugated probe for rat DAT (nucleotides 1153–2020; GenBank™ accession number NM_012694.2) and a digoxigenin-conjugated probe for rat Ctr9 (nucleotides 918–1794; GenBank™ accession number XM_238127.4). The generation of probes for *in vitro* transcription and cold *in situ* hybridization was performed as previously described (39). Once synthesized, the probes were added to the hybridization solution at a final concentration of 250 and 1500 ng/μl for DAT and Ctr9, respectively. Seventy microliters of hybridization solution were applied to each section, and the slides were cover-slipped and incubated for 16 h at 60 °C. The slides were washed and then treated with 20 μg/ml RNase A for 30 min. The slides were washed in decreasing salt concentrations (1× to 0.1× SSC) at room temperature and then at 60 °C in 0.1× SSC followed by a final rinse at room temperature in 0.1× SSC and distilled water. The slides were equilibrated to buffer A (100 mM Tris, 150 mM NaCl, 0.05% Tween 20, pH 7.5), then blocking was performed via incubation in blocking buffer for 1 h (buffer A containing 2% normal goat serum). Alkaline phosphatase-conjugated anti-Dig Fab fragments (Roche Applied Science) were diluted to 1:200 in blocking buffer and were applied for at least 16 h at 4 °C. Excess antibody was removed by washing in buffer A. The slides were then equilibrated to buffer B (100 mM Tris, 100 mM NaCl, 0.05% Tween 20, 50 mM $MgCl_2$, pH 9.4) for 10 min. The chromogen solution containing 5-bromo-4-chloro-3-indolyl phosphate and nitro blue tetrazolium salt (Roche Applied Science) was diluted at 2% in buffer B and applied in the dark; color development was monitored under a microscope. The reaction was terminated via the addition of 25 mM Tris, pH 8, and 5 mM EDTA, and the slides were rinsed in 1× TBS-Tween and incubated overnight in 1× PBS at 4 °C. The next day the slides were incubated in alkaline phosphatase-conjugated anti-fluorescein Fab fragments (Roche Applied Science) at a final concentration of 1:1000 overnight at 4 °C. Excess antibody was removed by washing in buffer A, and the slides were equilibrated in buffer B. Red colorimetric detection using 5-bromo-4-chloro-3-indolyl phosphate and 2-[4-iodophenyl]-3-[4-nitrophenyl]-5-phenyltetrazolium chloride (Roche Applied Science) was performed to visualize DAT (red staining). The images were acquired using a Zeiss Axiocam microscope.

Dopamine Uptake—Uptake experiments were performed as previously described (40) with some modifications. Briefly, the cells were transfected with a rat full-length DAT cDNA subcloned into pRcCMV (41) and plasmids for the pCis2 vector and Ctr9 full-length cDNA (subcloned into pCis2), which were generously provided by Dr. Stephen Desiderio (Johns Hopkins University). Forty-eight hours after transfection, the cells were

washed 3 times in uptake buffer (4 mM Tris base, 6.25 mM HEPES, 120 mM NaCl, 5 mM KCl, 1.2 mM $CaCl_2$, 1.2 mM $MgSO_4$, 1 mM ascorbic acid, and 5 mM glucose, pH 7.4). DAT-mediated uptake was measured after the incubation of cells for 7 min in 500 μl of uptake buffer containing 30 nM [^{3}H]DA (Amersham Biosciences and PerkinElmer Life Sciences) and increasing concentrations of unlabeled substrate (70–29,970 nM) to determine K_m and V_{max}. After incubation, the cells were washed 3 times with uptake buffer and then resuspended in 0.5 ml of 0.1 N NaOH. The entrapped radioactivity was counted via liquid scintillation spectrometry. Nonspecific DA uptake was determined by adding 100 μM nomifensine. The K_m and V_{max} values were determined via nonlinear regression analysis (GraphPad Prism software 5.0, San Diego, CA).

Cell Surface Biotinylation—Biotinylation was performed using the Cell Surface Protein Isolation kit (Pierce) according to the manufacturer's protocol. Briefly, the transfected BON cells were washed with PBS and incubated for 30 min at 4 °C in sulfo-NHS-SS-biotin in PBS. After terminating the reaction using the quenching solution, the cells were harvested and washed three times with TBS. The cells were lysed for 30 min at 4 °C with sonication every 5 min to improve solubilization and then centrifuged at 10,000 × *g* for 2 min. The supernatants were incubated in Neutravidin beads for 1 h at room temperature with rotation. After several washes, the samples were eluted in SDS-PAGE sample buffer containing 50 mM DTT for 1 h at room temperature. The samples were analyzed via Western blotting.

Results

Identification of Ctr9 as a DAT-interacting Protein—We used the yeast two-hybrid system to screen a rat brain library using the entire intracellular DAT-CT as bait. From several million transformants that were screened, 18 positive clones were found to encode partial sequences of the open reading frame of Ctr9, a 1173-amino acid protein containing 15 TPRDs and a Src homology-2 (SH2) domain.

To rule out the possibility of a false positive interaction, we tested several control constructs in the yeast two-hybrid system. Only transformants bearing the bait plasmid pP6-DAT-CT and the prey plasmid pP6-Ctr9 were positive for the β-galactosidase and the histidine phenotype selection. In addition to this screening, a yeast two-hybrid screen using the N terminus of DAT was performed in parallel, and no interaction between the N-terminal domain of DAT and Ctr9 was detected.

We next examined the specificity of this DAT-Ctr9 interaction by determining the ability of Ctr9 to bind to the C-terminal tail of the norepinephrine transporter (NET), a closely related SLC6a family member, using the yeast two-hybrid system. We found that Ctr9 also interacted with the intracellular C-terminal domain of NET. Although Ctr9 was the only TPRD-containing protein among all of the positive clones that interacted with DAT-CT, we assessed whether DAT-CT interacts with other proteins containing TPRDs. We subcloned the TPRD of two abundant proteins in the brain, cyclophilin 40 and protein phosphatase 5 (PP5), into the empty prey plasmid pP6. Using the two-hybrid system, we failed to observe any interaction between DAT-CT and cyclophilin 40 or protein phosphatase 5, thus demonstrating the specificity of the association between DAT-CT and Ctr9 (Fig. 1*A*).

Mapping the Interaction Domain of DAT—To determine which regions of DAT are involved in the formation of the DAT-Ctr9 complex, we assessed the ability of various portions of DAT-CT to interact with Ctr9 using the yeast two-hybrid system. A first series of four constructs with successive deletion in the 3′-end of DAT-CT were tested. As shown in Fig. 1*B*, the second half of the DAT-CT is not involved in this interaction. DAT-Ctr9 complex formation appears to be dependent only interaction with the first 24 amino acids of DAT-CT (Tyr^{574}-Glu^{597}). Interestingly, this first half of DAT-CT contains a motif (FREKLAYAIA) that was determined to be essential for constitutive DAT-mediated and PKC-stimulated internalization processes (22, 42, 43). The disruption of this motif in the Δ32-CT mutant suppressed this interaction.

To more precisely define the critical amino acids required for the putative interaction between DAT and Ctr9, we inserted amino acid mutations into the first half of DAT-CT. As depicted in Fig. 1*C*, single, double, or triple point mutations in the amino acid sequence of the FREKLAYA motif (E588A, L590S, A591E, Y592R/A592S, or R587A/E587A/K587A) exerted no effect on the binding of DAT to Ctr9. Similarly, the strength of this interaction was preserved despite the mutation of the residues Pro^{583}, Gly^{584}, Leu^{590}, Ile^{594}, and Glu^{597}, whereas a decreased interaction strength was observed when residues Tyr^{577}, Lys^{578}, and Phe^{579} were mutated. Nevertheless, none of these single mutations abolished the DAT Ctr9 interaction.

Amino acid sequence analyses of DAT and NET, both of which interact with Ctr9, revealed a high sequence identity of the first six amino acids of the C-terminal tail. Indeed, the deletion of these six residues led to the complete suppression of DAT-Ctr9 binding (Fig. 1*B*). We then tested constructs in which the Tyr^{577}, Lys^{578}, and/or Phe^{579} (YKF motif) residues were mutated to Ala^{577}, Ala^{578}, and Ser^{579}, respectively (AAS motif). No interaction was observed with the triple mutant Y577A/K577A/F577S (DAT_{AAS}), but a very weak interaction signal was detected for the double mutant (Y577A/K577A). Taken together, these results indicated that the YKF motif (residues 577–579) is critical for DAT-Ctr9 complex formation.

Identification of the Interaction Domains of Ctr9—Ctr9 contains 15 TPRDs that are able to mediate coiled-coil interactions. Primary sequence alignment between the 18 clones found in the original screen and full-length Ctr9 allowed us to identify a contig sequence that comprises TPRD6 through TPRD12, *i.e.* ~1000 bp. To delineate the interacting domains, we initially constructed a series of Ctr9 mutants in which the 5′-end was successively deleted. As shown in Fig. 2*A*, the deletion of TPRD6 or more resulted in the loss of the interaction between DAT and Ctr9. We next tested a second series of constructs in which the 3′-end of Ctr9 was successively deleted. It appeared that the TPRDs in 3′-end of TPRD10 are not required for the binding of Ctr9 to DAT (Fig. 2*B*). We then refined these results by testing the effects of deleting one- or two-thirds of these TPRDs 6 and 10. We found that the region containing the final seven amino acids of TPRD6 to the first eight residues of

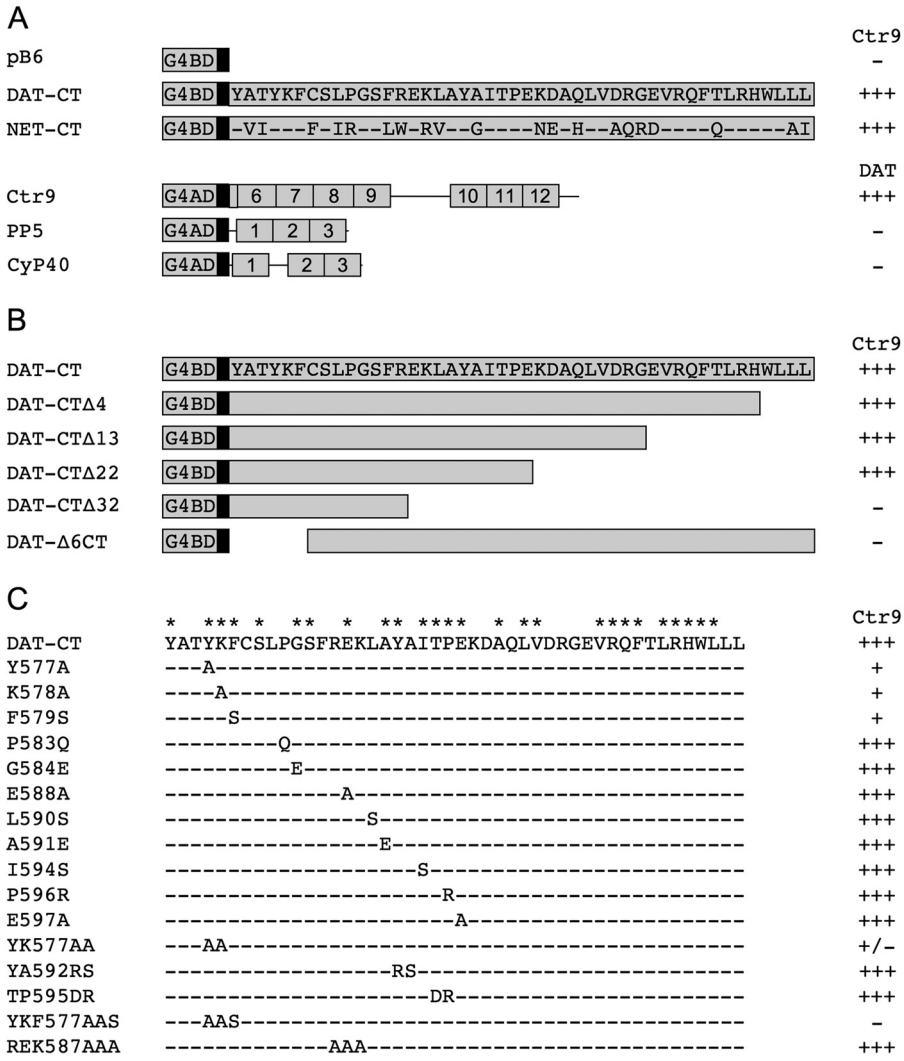

FIGURE 1. **Identification of the amino acids of DAT required for the DAT-Ctr9 interaction via a yeast two-hybrid assay.** *A*, schematic representation of the bait (*upper panel*) and prey (*lower panel*) cDNAs fused to the GAL4 binding (*G4BD*) and activation domains (*G4AD*), respectively. Note that Ctr9 binds to the C termini of DAT and NET. No interaction was detected for the TPRD-containing proteins phosphatase 5 (*PP5*) and cyclophilin 40 (*CyP40*), demonstrating the specificity of the DAT-Ctr9 interaction. *B*, the deletion of DAT-CT. Domain delimitation revealed the importance of the first third of DAT-CT. *C*, point mutagenesis of DAT-CT emphasized that residues YKF are required for the DAT-Ctr9 interaction. * represents the conserved amino acids between DAT and NET.

TPRD10 is necessary and sufficient to bind the intracellular DAT-CT (Fig. 2*C*).

Taken together these data demonstrated that DAT-Ctr9 complex formation is mediated by a direct protein-protein interaction between the membrane-proximal portion of the intracellular tail of DAT and a 500-bp region of Ctr9 that contains the three complete TPRDs, TPRD7, -8, and -9.

Three-dimensional Modeling of the DAT-Ctr9 Interaction—The original aim of the modeling studies was to characterize the binding interface between DAT-CT and the TPRD region of Ctr9. Another aim was to generate a potential tool to explain the previously obtained mutagenesis results. The primary step in the generation of a homology model is sequence alignment (blast) between the protein of interest and a previously crystallized protein (typically from the Protein Date Bank).

Considering the results obtained from yeast two-hybrid screening and the lack of relevant templates for the entire DAT and Ctr9 sequences, we focused on DAT-CT and the Ctr9 region from the beginning of TPRD5 to the end of TPRD10 (90% of the contig). The scoring function used for alignment was Blosum62 in the case of the DS protocol. Blasts were performed against the PDB database to identify a potential crystal structure. The different results were compared and manually analyzed. Secondary structure predictions were performed on the entire structure, which appeared to be crucial for template selection. Indeed, because we did not select the entire protein for homology modeling, we selected a template according to secondary structure information (PDB and predicted structures). In addition to the partially crystallized DAT-CT (PDB code 4M48), only two sequences appeared to be relevant to DAT-CT: alanine racemase (PDB code 1VFH) and MoeA (PDB code 2NQS). Concerning Ctr9, the best template was the crystallized TPRD from *O*-linked GlcNAc transferase (PDB code 1W3B).

During alignment sequence refinement, we observed a high degree of homology between a Ctr9 region in which no TPRD had previously been identified (between TPRD9 and -10) and the TPRD of the template (Fig. 3*A*). A precise comparison of the

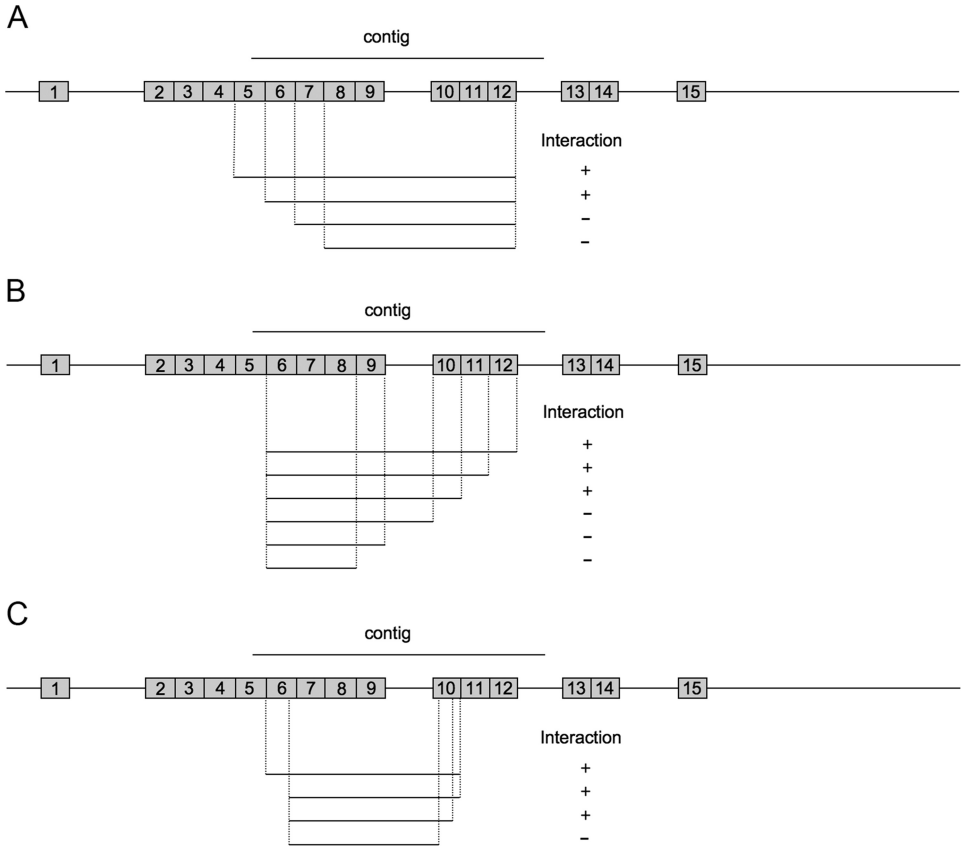

FIGURE 2. **Involvement of a 500-bp region of Ctr9 consisting of TPRD6 to TPRD10 in the DAT-Ctr9 interaction.** Ctr9 is represented as a scaled map in which its 15 TPRDs are displayed as *filled boxes*. The *lines under the Ctr9 map* denote the different regions tested for their interaction with DAT in the yeast two-hybrid experiments. *A*, successive 5′ deletions of the Ctr9 contig sequence, which indicated that the region before TPRD6, is not necessary for the DAT-Ctr9 interaction. *B*, successive 3′ deletions of the Ctr9 sequence, which indicated that the region after TPRD10 is not necessary for the DAT-Ctr9 interaction. *C*, refinement of the minimal Ctr9 region required for its interaction with DAT.

Ctr9 sequence to the known TPR consensus sequence revealed a novel TPRD in this region, termed TPRD9b. Two additional TPRDs between the N terminus and TPRD1 and between TPRD14 and TPRD15 were identified and termed TPRD1b and -14b, respectively (Fig. 3*B*). Thus, Ctr9 appears to contain 18 TPRDs rather than the 15 TPRDs originally described (24).

After model generation (50 models/protein) and selection (energy-based), we processed the docking of the best homology model of Ctr9 to that of DAT-CT, which was used as a receptor. We generated ~2000 poses clustered according to their distances and interaction energies. The most representative clusters (Fig. 3*C*) were analyzed, and the interaction on a specific portion of DAT-CT was highlighted. We selected the best pose in these clusters according to the quality of the complex structure (Fig. 3*D*; Ref. 36).

Validation of the DAT-Ctr9 Complex Model—To evaluate the different interactions observed during the docking step, we validated our docking model using the mutagenesis results (Fig. 1*C*). We were able to differentiate the mutations into two categories: mutants affecting recognition and residues without any effect. For Y577S, little information could be examined due to its proximity to the membrane. However, Tyr^{577} appeared to be important for DAT-CT helix orientation, and Y577S seemed to alter the DAT helix orientation due to a loss of the π-cation interaction of the aromatic side chain of Tyr^{577} with the Lys^{139} ammonium of the third DAT transmembrane domain. The hydroxyl side chain of Tyr^{577} could also interact with the hydroxyl group of Ser^{581} to form a hydrogen bond (Fig. 3*E*, *left panel*). The K578A mutation led to the loss of multiple intraactions (DAT/DAT) and interactions (DAT-Ctr9). Indeed, the hydrophobic chain of this lysine residue predominantly interacted with the side chain of Leu^{582} of DAT and facilitated its extension to the Asp^{426} carboxylate of CTR9 (TPRD9). This positioning induced the formation of an electrostatic bond between the carboxylate and the ammonium of Asp^{426} and Lys^{578}, respectively. Different hydrogen bonds between the ammonium of Lys^{578} and the backbone of both DAT and CTR9 were also detected. For example, Lys^{578} ammonium bound to the carbonyl backbone of both Thr^{425} and Gln^{424} (TPRD9) via hydrogen bonds (Fig. 3*E*, *middle panel*). Residue Phe^{579} was stabilized in its conformation via a σ-π interaction with the methyl side chain of Ctr9 Thr^{425} (TPRD9; Fig. 3*E*, *right panel*). As for the DAT amino acids for which mutation exerted no effect, we found that all of these residues were outside the predicted binding interface. Overall, *in silico* analysis of our DAT-Ctr9 interaction model explained the results obtained from the yeast two-hybrid experiments, which in turn validated our three-dimensional representation of the DAT-Ctr9 complex.

Co-expression and Co-localization of DAT and Ctr9—To interact with each other, proteins must co-localize within the same cell. To validate this point, immunohistochemistry is commonly used. However, in our hands commercially available

Ctr9 antibodies failed to provide specific labeling in either brain tissue slices or Ctr9-transfected cells. Therefore, we used HA- or myc-tagged Ctr9 (mouse full-length) to determine the subcellular localization of Ctr9 and whether it co-localized with DAT. As previously described (24), Ctr9 displayed a strong nuclear expression (*arrowheads*; Fig. 4, *A* and *B*), in the majority of transfected cells. Interestingly, in some cells Ctr9 was detected outside the nucleus (*arrows*, Fig. 4, *A* and *B*). Subse-

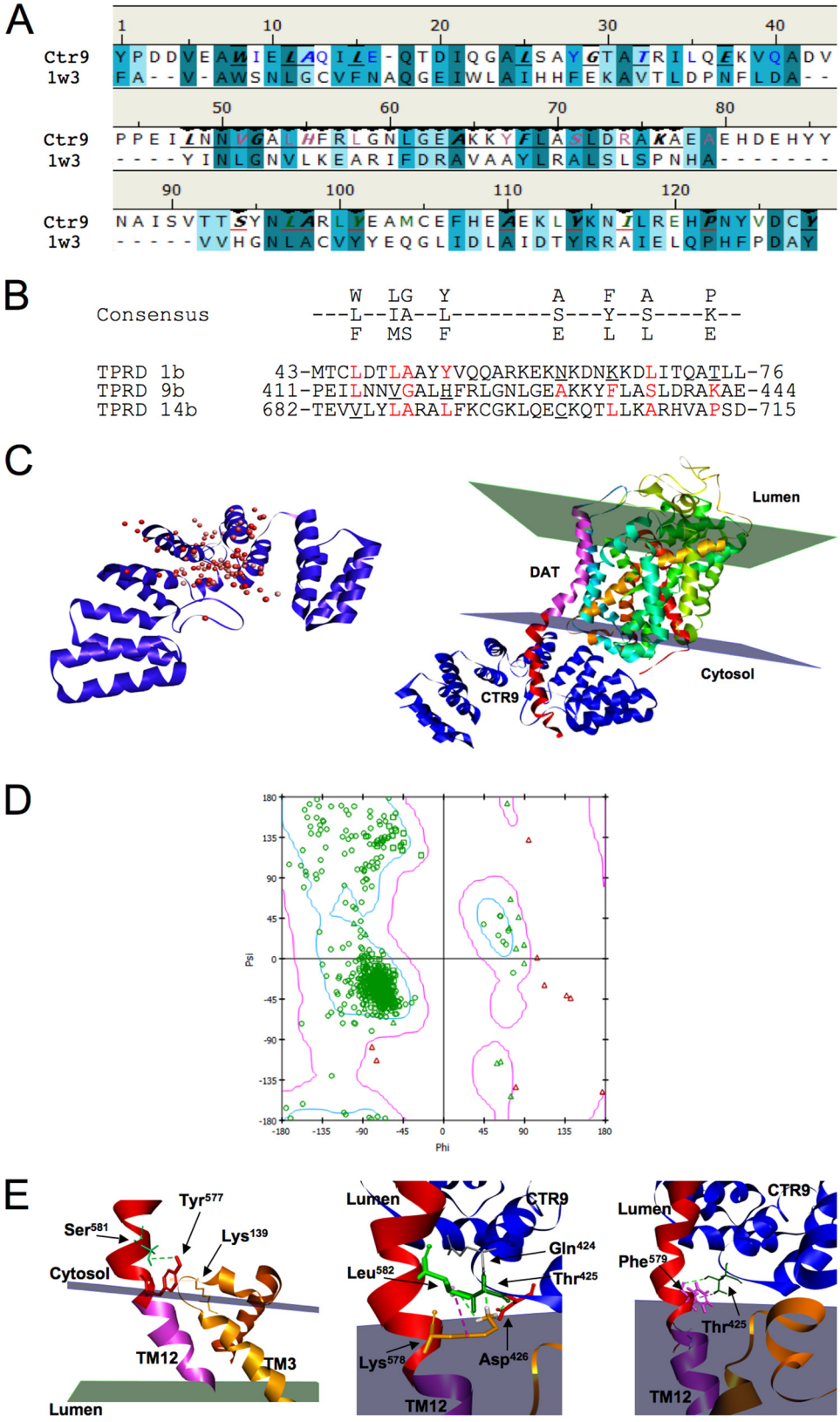

quently, we examined if Ctr9 co-localized with DAT by co-expressing myc-tagged Ctr9 and human DAT in BON cells. Neither myc-tagged Ctr9 nor DAT was detected in the mock-transfected cells (data not shown). As expected, DAT protein was detected at the plasma membrane with some labeling in the cytoplasm. Fig. 4*E* displayed an overview of transfected cells, showing cells that expressed only Ctr9 (*arrowheads*) or both Ctr9 and DAT (*arrows*). In these last cases, particularly in cells with extended processes, Ctr9 partially co-localized with DAT in the cytoplasm and in the close vicinity of the plasma membrane, as illustrated in Fig. 4*F*.

We next examined whether DAT forms a complex with Ctr9 in cells co-expressing both proteins via co-immunoprecipitation. As depicted in Fig. 4*C*, immunoprecipitation of DAT using an anti-DAT antibody resulted in the co-precipitation of Ctr9. The Ctr9 protein is composed of two primary domains, the TPRD and the SH2 domain. In the yeast two-hybrid experiments, we showed that the SH2 domain was not required for the interaction of DAT with Ctr9. We thus generated a HA-tagged Ctr9 construct lacking the SH2 domain, containing amino acids 1–831 (15 residues after the final TPRD) and designated HA-Ctr9ΔSH2. Immunoprecipitation using an anti-HA antibody resulted in the co-precipitation of DAT in the cells transfected with both DAT and HA-tagged Ctr9ΔSH2 (Fig. 4*D*). These results provided evidence for an interaction between DAT and either full-length or truncated Ctr9.

As Ctr9 antibodies were not suitable to directly detect the co-localization of DAT and Ctr9 proteins *in vivo* via immunohistochemistry, we investigated whether their mRNAs were co-expressed in the same neurons. To this aim, double-labeling *in situ* hybridization was performed using fluorescein- and digoxigenin-labeled riboprobes for DAT and Ctr9, respectively. As previously described (41), DAT expression was restricted to the substantia nigra *pars compacta* and the ventral tegmental area (VTA, Fig. 4*G*, *middle panel*). The Ctr9 expression profile was more ubiquitous, including stronger expression in the hippocampus (Fig. 4*G*, *left panel*) and the cortex, brain areas containing a high density of cell bodies. However, Ctr9 expression was clearly detected in dopaminergic regions and specifically in DAT-positive neurons (Fig. 4*G*, *middle panel*), supporting that Ctr9 is an endogenous DAT binding partner.

Finally, we assessed whether DAT and Ctr9 can form a protein complex *in vivo* via co-immunoprecipitation using mouse striatal, substantia nigra *pars compacta*, and VTA tissues. As shown in Fig. 4*H*, DAT was co-immunoprecipitated using the anti-Ctr9 antibody, but not rabbit IgG, from extracts from wild-type animals, indicating an interaction between DAT and Ctr9. This DAT-Ctr9 association was confirmed by a pulldown assay using a GST fusion protein containing the 1000-bp contig region of Ctr9 (TPRD6 through TPRD12). As shown in Fig. 4*I*, GST-Ctr9 precipitated DAT from the striatum of wild-type mice. In control studies, DAT was not detected in DAT knock-out mice or using GST alone. Taken together, these results confirm the existence of a protein complex containing DAT and Ctr9 and clearly demonstrate that Ctr9 can strongly interact with the native DAT.

Effect of Ctr9 on DAT Activity—DAT plays a critical role in the regulation of dopaminergic neurotransmission and synaptic strength. Because DAT is the primary mechanism by which DA is rapidly cleared from the synaptic cleft, changes in its function should thus modify the synaptic DA concentrations. As we established a physical interaction between DAT and Ctr9, we analyzed the effect of Ctr9 overexpression on DA uptake activity in transfected BON cells.

DAT-mediated [^{3}H]DA uptake was significantly increased in BON cells co-transfected with the Ctr9 expression vector compared with cells co-transfected with the empty expression vector pCis2 (Fig. 5*A*). The enhancement of DA uptake by Ctr9 corresponds to an increase in the translocation velocity of cellular DA, with an estimated 50% increase in V_{max} for DAT-mediated [^{3}H]DA uptake (DAT/pCis2: 15.8 ± 0.99 pmol/mg/min; DAT-Ctr9: 25.28 ± 2.45 pmol/mg/min). No significant difference in the affinity of DA for the transporter was observed between the DAT-Ctr9-co-expressing cells and the cells expressing DAT alone (DAT/pCis2: K_m = 1.62 ± 0.38 μM; DAT-Ctr9: K_m = 1.93 ± 0.30 μM). DAT-mediated DA uptake was completely inhibited (>95%) by 100 μM nomifensine, a transporter blocker, whereas in mock-transfected cells (vector DNA) or in cells expressing Ctr9 alone, no DA uptake was observed (data not shown). These data suggested that the enhancement of DAT activity in the presence of Ctr9 is likely not due to changes in the intrinsic properties of DAT (such as the turnover rate or the recognition of DA by the DAT ligand binding domain) but rather to an increase in the number of transporters expressed at the plasma membrane.

As Ctr9 is endogenously expressed in human BON cells, we ascertained whether the up-regulation of DAT uptake is specifically due to Ctr9 overexpression. We co-transfected cells with DAT, Ctr9, and either a scrambled shRNA (shScr) or an shRNA against mouse Ctr9 (shm). The expression of shScr did not affect DAT uptake activity in either the presence or absence of Ctr9. Indeed, Ctr9 induced a 57% increase in V_{max} (DAT/shScr: 11.87 ± 0.46 and DAT-Ctr9/shScr: 18.63 ± 0.61 pmol/mg/min), with no significant changes in DAT affinity (Fig. 5*B*). No significant difference in DAT-mediated [^{3}H]DA uptake was observed between transfection with shm and shScr in the

FIGURE 3. **Three-dimensional model of the DAT-Ctr9 complex.** *A,* sequence alignment of Ctr9 (TPRD9 to TPRD10) with *O*-linked GlcNAc transferase (PDB code 1w3b). The *blue tones* (from *light to dark blue*) represent the increasing degree of residue similarity and indicate a novel TPRD (*middle lane*) between TRPD 9 and TPRD10. *B,* the primary sequences of the consensus TPR and the newly identified TPRD in Ctr9. The *red* and *underlined residues* indicate the conserved and non-conserved amino acids, respectively. The *numbers at the sides* refer to the position of each sequence in the protein. *C*, three-dimensional representation of Ctr9 from TPRD6 to TPRD11 (*blue*) and DAT (transmembrane and C-terminal tail domains). *Left panel*, schematic representation of the different docking clusters of DAT to CTR9 (the *red spheres*, from *light to dark*, represent the most representative clusters) using the protein docking module (ZDock and Rdock, DS Modeling 2.5 software). *Right panel*, three-dimensional model of Ctr9 (*blue*) interacting with DAT. The three-dimensional structure of DAT was generated using PDB entries 1VFH and 2NQS and the partially crystallized DAT-CT (PDB entry 4M48) as templates. *D*, Ramachandran plot (62) of DAT/CTR9 complex. *Green and pink zones* delimit tolerated regions. To the exception of glycine residues (indicated by the *green triangles*) all residues (*green circles* and *squares*) are included in favorable conformation regions. *E,* validation of our model using mutagenesis data. The three-dimensional model of the interaction between DAT amino acids Tyr^{577} (*right*), Lys^{578} (middle) and Phe^{579} (*left*) and the Ctr9 residues.

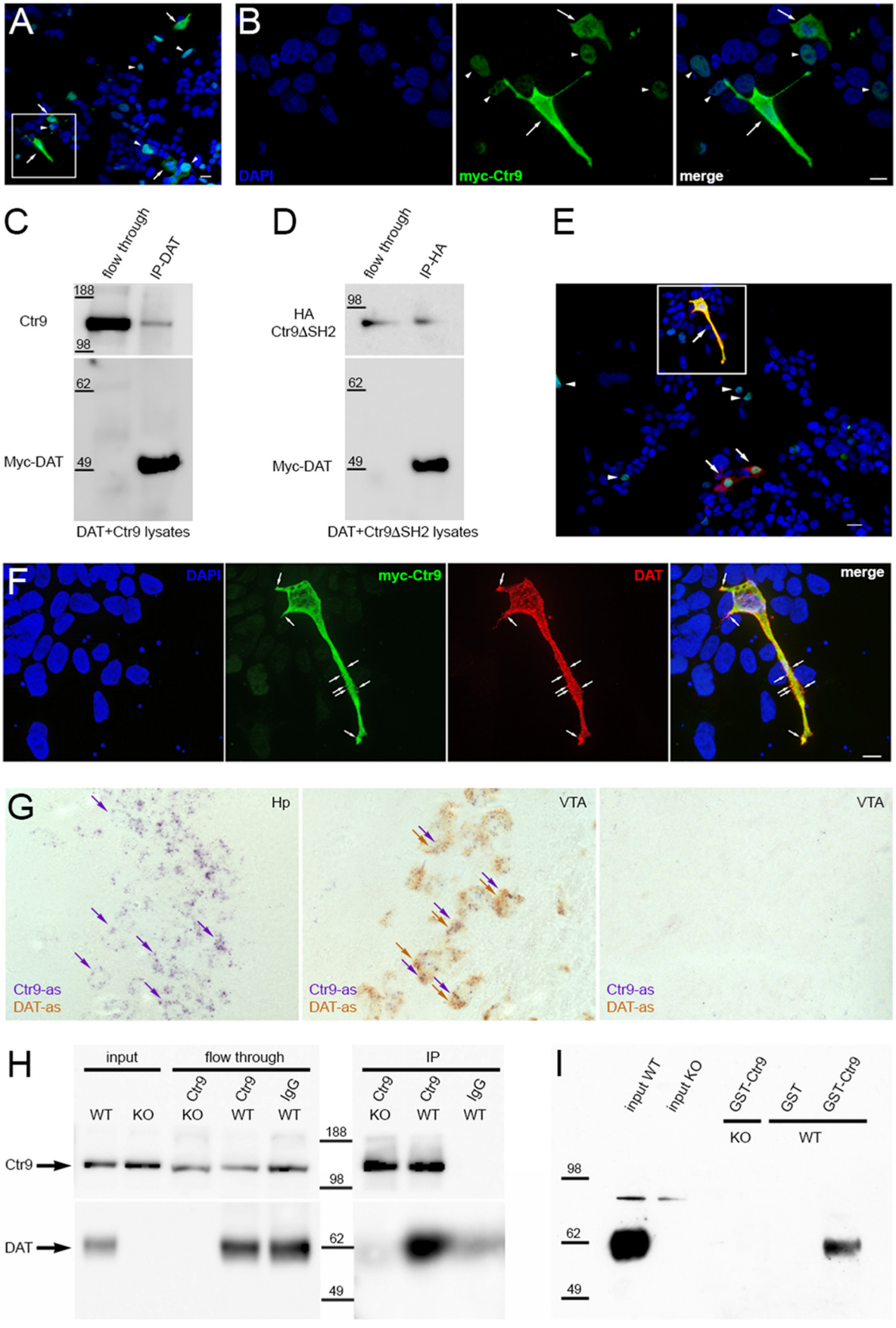
A
B
DAPI
myc-Ctr9
merge
C
flow through
IP-DAT
188
98
Ctr9
62
49
Myc-DAT
DAT+Ctr9 lysates
D
flow through
IP-HA
98
HA
Ctr9ΔSH2
62
49
Myc-DAT
DAT+Ctr9ΔSH2 lysates
E
F
DAPI
myc-Ctr9
DAT
merge
G
Hp
VTA
VTA
Ctr9-as
DAT-as
Ctr9-as
DAT-as
Ctr9-as
DAT-as
H
input
flow through
IP
WT
KO
Ctr9
KO
Ctr9
WT
IgG
WT
Ctr9
KO
Ctr9
WT
IgG
WT
188
98
Ctr9
62
49
DAT
I
input WT
input KO
GST-Ctr9
KO
GST
GST-Ctr9
WT
98
62
49

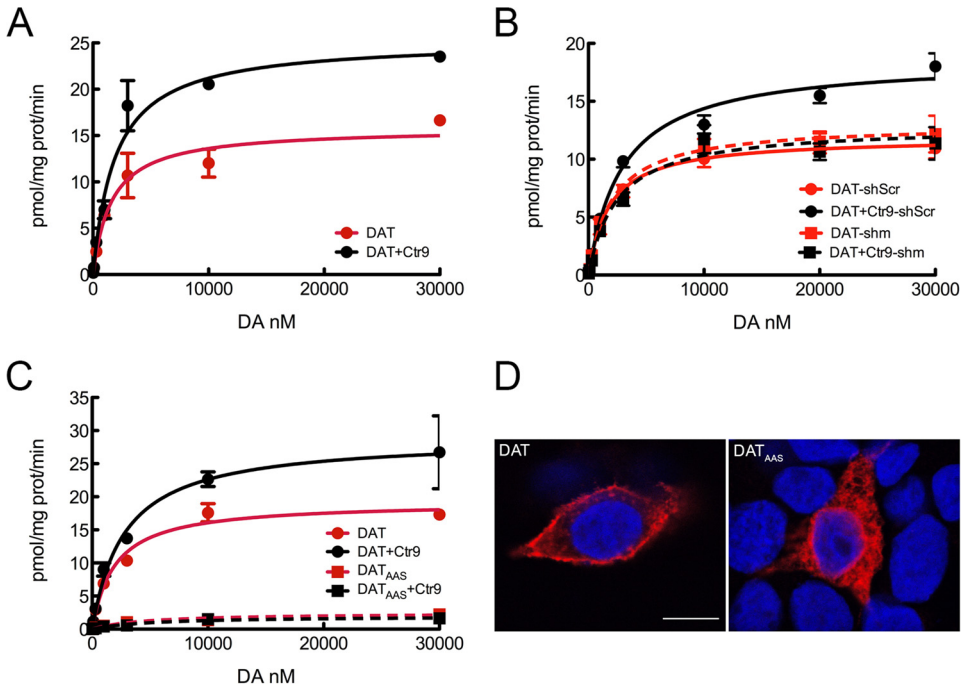

FIGURE 5. **The regulation of DAT activity by Ctr9.** *A*, [^{3}H]DA uptake activity in cells transfected with DAT alone or in combination with Ctr9. DAT activity (V_{max}) was increased in the presence of Ctr9. *B*, the enhancement of [^{3}H]DA uptake in the presence of Ctr9 was completely abolished using an shRNA against mouse Ctr9 but not using a scrambled shRNA. The graph displays the means ± S.E. of three separate experiments performed in triplicate. *C*, the mutation of DAT residues YKF results in a 90% decrease in DAT activity and the loss of potentialization by Ctr9. *A* and *C*, the graphs display the means ± S.E. of the results of one triplicate transfection representative of five and three independent experiments, respectively. *D*, impaired localization of the DAT$_{AAS}$ mutant. The Y577A/K577A/F577S mutation induced the sequestration of DAT in the cytoplasm. Immunochemistry was performed using our rabbit polyclonal anti-DAT antibody (*red*), and the nuclei were labeled with DAPI (*blue*). The individual cells displayed are representative of the entire cell population from three independent experiments performed in duplicate. *Scale bar*: 10 μm.

absence of Ctr9. By contrast, the expression of shm completely abolished the effect of Ctr9 on DAT activity (DAT/shm: 13.04 ± 0.58 pmol/mg/min; DAT-Ctr9/shm: 12.87 ± 0.72 pmol/mg/min), confirming that the up-regulation of DA uptake was specifically mediated by Ctr9 over-expression.

Effect of the Y577A/K577A/F577S Mutation on DAT Activity and Targeting—As described above, DAT-Ctr9 complex formation absolutely requires the presence of the intact YKF motif of DAT based on yeast two-hybrid experiments. We thus examined the effect of the replacement of YKF with AAS on DAT activity in cells in the presence or the absence of Ctr9 overexpression. We found that DAT$_{AAS}$ displayed a significant decrease (~90%) in DA uptake activity compared with wild-type DAT (Fig. 5*C*). More importantly, Ctr9 overexpression did not enhance the residual DA uptake mediated by DAT$_{AAS}$ (Fig. 5*C*).

Changes in plasma membrane transporter uptake activity have frequently been shown to result from changes in transporter subcellular localization. For instance, it has been demonstrated that the alteration of DAT activity mediated by interactions with protein partners or by pharmacological substances occurs as a consequence of enhanced DAT recruitment to the plasma membrane or DAT sequestration in the cytoplasm (14, 8, 44). To determine whether the dramatic reduction in DAT activity observed for DAT$_{AAS}$ is due to the altered localization of the mutant transporter, we performed immunocytochemistry on wild-type and mutant DAT-transfected cells. As illustrated in Fig. 5*D*, wild-type DAT predominantly localized to the plasma membrane of these cells. The mutation of the YKF motif resulted in a redistribution of this transporter to the cytoplasm, consistent with the 90% decrease in DAT-mediated DA uptake. These results demonstrated the crucial and unspecified role of

FIGURE 4. **Co-expression and co-localization of DAT and Ctr9.** *A* and *B*, Ctr9 expression in BON cells transfected with a Myc-tagged full-length Ctr9. The Ctr9 protein predominantly localized to the nucleus (*arrowheads*), but in some cells Ctr9 expression was present in the cytoplasm and the close vicinity of the membrane (*arrows*). *C* and *D*, Ctr9 or DAT was immunoprecipitated (*IP*) from BON cells transfected with DAT and Ctr9 (*C*) or Ctr9ΔSH2 (*D*). The results showed that DAT can form a complex with either full-length Ctr9 or Ctr9ΔSH2. *E* and *F*, co-expression of DAT and Myc-tagged Ctr9 in BON cells. Note the co-localization of DAT (*red*) and Ctr9 (*green*) at the plasma membrane in cells with processes (*arrows*), whereas in more rounded cells (*arrowheads*), Ctr9 is localized in the nucleus (labeled with DAPI, blue). *A*, *B*, *E*, and *F*, immunochemistry was performed using our rabbit polyclonal or a rat monoclonal (Chemicon) anti-DAT antibody (*red*) and a mouse monoclonal anti-Myc antibody (Clontech). Images were acquired using a Zeiss Apotome microscope at ×20 (*A* and *E*, *scale bar*: 20 μm) or ×63 (*B* and *F*, *scale bar*: 10 μm) magnification. *G*, double-labeling *in situ* hybridization revealed that Ctr9 (digoxigenin, *purple arrows*) and DAT (fluorescein, *orange arrows*) are co-expressed in dopaminergic neurons *in vivo*. *Left panel*, in the hippocampus (*Hp*), where no DA-expressing neurons are present, only Ctr9 mRNA was detected. *Middle panel*, Ctr9 is expressed in all dopaminergic (DAT-positive) neurons in the VTA. *Right panel*, no hybridization signal was observed in the VTA using DAT and Ctr9 sense probes. *Scale bar*: 100 μm. *H*, DAT co-precipitates with Ctr9. Immunoprecipitations were performed from mouse tissue (from the striatum, the VTA, and the substantia nigra *pars compacta*) using an anti-Ctr9 antibody or rabbit IgG as a control. *I*, the GST-Ctr9 fusion protein can precipitate full-length DAT. Aliquots containing GST alone or GST-Ctr9 were incubated in striatal synaptosomal lysates from wild-type or DAT knock-out mice, and the precipitated proteins were analyzed via Western blotting using the anti-DAT antibody. The *input* lanes were loaded with 5 μg of the striatal synaptosomal lysates.

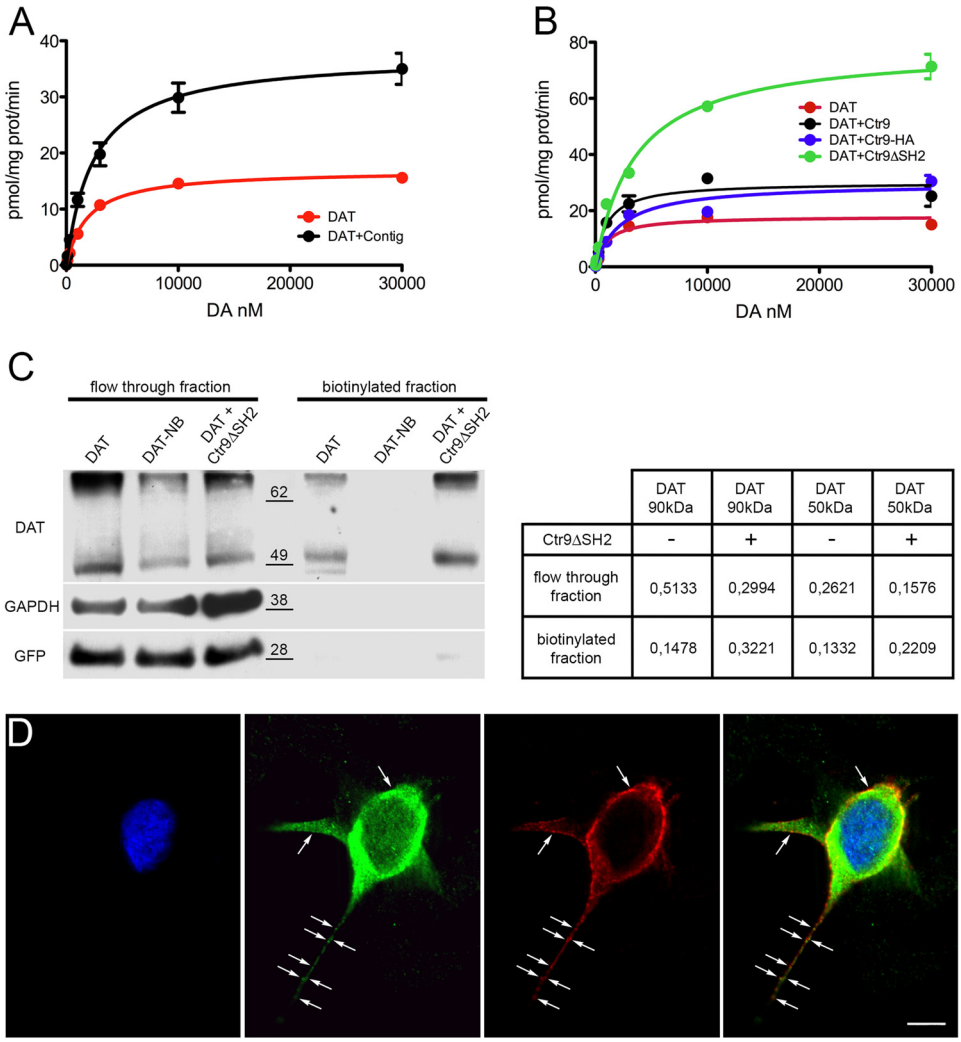

	DAT 90kDa	DAT 90kDa	DAT 50kDa	DAT 50kDa
Ctr9ΔSH2	-	+	-	+
flow through fraction	0,5133	0,2994	0,2621	0,1576
biotinylated fraction	0,1478	0,3221	0,1332	0,2209

FIGURE 6. **The Ctr9-mediated regulation of DAT does not require the SH2 domain of Ctr9.** *A*, [^{3}H]DA uptake activity in cells transfected with DAT alone or in combination with the Ctr9 contig containing TPRD6 to TPRD12. The graph displays the means ± S.E. of four separate experiments performed in triplicate. *B*, [^{3}H]DA uptake activity in cells transfected with DAT alone or in combination with full-length Ctr9 (untagged or HA-tagged) or HA-tagged Ctr9ΔSH2. DAT activity (V_{max}) was enhanced in the presence of either protein. The graph displays the means ± S.E. of three separate experiments performed in triplicate. *C*, biotinylation experiments in cells transfected with DAT alone or in combination with Ctr9ΔSH2. *Left panel*, the transfected cells were incubated in sulfo-NHS-SS-Biotin, and the labeled proteins were analyzed via Western blot using a rat anti-DAT antibody (Chemicon), a mouse anti-GAPDH (Calbiochem), or a rabbit anti-GFP (Life Technologies). *Right panel*, the immunoblots from the biotinylation experiment were scanned using a LAS-3000 imager and were quantified using MCID software. The values are expressed as the relative optical densities. *D*, immunochemistry was performed using a mouse monoclonal anti-Myc antibody (for Ct9, *blue*), a rat anti-HA antibody (for Ctr9ΔSH2, *green*), and our rabbit polyclonal anti-DAT antibody (*red*). The *white arrows* denote the co-localization of Ctr9ΔSH2 and DAT at the plasma membrane. The individual cells displayed are representative of the entire cell population from three independent experiments performed in duplicate. *Scale bar*: 10 μm.

amino acids Tyr^{577}, Lys^{578}, and Phe^{579} of DAT in its subcellular localization and indirectly suggest that Ctr9 is involved in DAT recruitment to or stabilization in the plasma membrane.

Compartmentalization of Ctr9 and the Role of the SH-2 Domain—We demonstrated that Ctr9 can interact with DAT, leading to changes in DAT activity. We have also shown that the binding of Ctr9 to DAT requires a minimal TPRD-containing region of ~500 bp of Ctr9. However, the results we obtained from whole-cell expression do not completely rule out the possibility that the effects of Ctr9 are established in the nucleus via direct changes in transcriptional activity via the activation of the transcription complex Paf1. We next aimed to directly compete with the protein-protein interaction between Ctr9 and DAT using a variety of interfering peptides. These peptides were derived from the DAT sequence YATYKFCSLPGS-FREKL, which was fused to either the HIV TAT sequence or an isoprenylated moiety (45). These peptides at low doses completely reversed the Ctr9 expression-induced increase in V_{max} (not shown), but we obtained similar results using the scramble peptide controls. We believe that the TAT sequence directly interfered with the DAT-Ctr9 coiled-coil interaction, confounding our results. Therefore, it remained necessary to clearly establish that our results were not a consequence of transcriptional changes.

In an initial set of experiments, we directly used the contig (TPRD6–12), and we showed that this small protein up-regulated DAT activity (Fig. 6*A*), with a 125% increase in V_{max} (DAT/pCis2: 16.94 ± 0.37 pmol/mg/min; DAT/contig: 37.46 ± 1.79 pmol/mg/min, $p < 0.001$) and that Ctr9 (tagged or not) induced a 60% increase in V_{max}. The second set of experiments

was performed using Ctr9ΔSH2, which lacked the SH2 domain, whose function in Ctr9 was not identified. We transfected BON cells with DAT in the presence or absence of Ctr9ΔSH2. As for the contig, [^{3}H]DA uptake was increased in the cells co-expressing DAT and Ctr9ΔSH2 compared with the cells transfected with DAT alone. The determination of the kinetic parameters showed that this augmentation was due to a change in V_{max} (DAT: 18.01 ± 0.84 pmol/mg/min; DAT-Ctr9ΔSH2: 78.38 ± 2.45 pmol/mg/min, $p < 0.001$). This V_{max} augmentation was stronger for Ctr9ΔSH2 (334%) than for the contig or Ctr9 (tagged or not). No significant modification of K_m (Fig. 6*B*) was observed, suggesting that Ctr9 modulates the number of transporters at the plasma membrane.

To address this issue, we performed cell surface biotinylation using sulfo-NHS-SS-biotin. Unbiotinylated control membranes (DAT-NB) showed no binding to the avidin-agarose beads. Western blotting using an anti-DAT antibody revealed two bands at ~50 and 75/80 kDa (Fig. 6*C*, *left panel*), which is consistent with the coexistence of DAT in both its immature and fully mature forms (10, 46, 47). As an immature band should not normally be on the cell surface and, therefore, should not get biotinylated, we verified the lack of biotinylation of two intracellular protein GFP (co-transfected) and GAPDH (endogenously expressed), ensuring the accuracy of our experiments and results. Quantitative analysis revealed that under conditions in which the total levels of transporter expression remained unchanged, the cells co-expressing DAT and Ctr9ΔSH2 exhibited a higher level of DAT expression at the cell surface (biotinylated DAT/total DAT: 104%; biotinylated DAT/flow-through: 227.79%) compared with the cells expressing DAT alone. However, this increase was not equivalent between the two forms of DAT. Cell surface expression was up-regulated by 130 and 75% (biotinylated DAT/total DAT) for the 75/80- and 50-kDa bands, respectively. For the biotinylated DAT/flow-through ratio, we observed an increase of 273 and 175% in the 75/80- and 50-kDa bands, respectively (Fig. 6*C*, *right panel*).

Finally, we examined the subcellular expression of HA-tagged Ctr9ΔSH2 compared with the full-length Myc-tagged Ctr9 in the presence or absence of DAT. Surprisingly, immunocytochemistry revealed that the deletion of the SH2 domain resulted in a dramatic loss of Ctr9 nuclear localization (Fig. 6*D*), a finding that is interesting in and of itself because it indicates a role of this domain in the intranuclear targeting of the protein. Indeed, Ctr9ΔSH2 was almost exclusively localized to the cytoplasm and was partially co-localized with DAT at the plasma membrane (Fig. 6*D*). Taken together, these results indicated that Ctr9-enhanced DAT-mediated DA uptake does not require the presence of the SH2 domain-mediated nuclear localization of Ctr9.

Discussion

In the present study we identified Ctr9, a TPRD-containing protein, as a novel regulator of DAT activity. We demonstrated that Ctr9 directly interacts with DAT based on yeast two-hybrid experiments and pulldown assays. Furthermore, we confirmed this interaction via co-immunoprecipitation, immunocytochemistry, and *in situ* hybridization, showing that Ctr9 co-localizes with DAT in neurons and cells and up-regulates DAT uptake activity by >50%. Finally, this study revealed that Ctr9, previously described as a nuclear protein belonging to the transcription complex Paf1, plays an unexpected functional role in the neuronal cytoplasm.

A Role of the DAT-CT Residues YKF in DAT Trafficking—DAT interaction with Ctr9 was mediated by the DAT-CT and, more precisely, via a core motif of the three amino acids Tyr^{577}-Lys^{578}-Phe^{579}. The mutation of these residues led to a dramatic decrease in DA uptake, which was associated with the altered subcellular localization of the transporter, *i.e.* the sequestration of DAT in the cytoplasm. These results suggest a role of the YKF motif in DAT trafficking and localization. Studies identifying the molecular determinants regulating transporter trafficking have primarily noted the requirement of the second half of the DAT-CT sequence for the appropriate folding and the effective endoplasmic reticulum (ER) export of the transporter. A deletion in the hDAT C terminus, from residue 591 to the end, abolished transporter function (<1% of the wild-type transporter) due to the altered targeting of this mutant (48). Specifically, the deletion of the hDAT PDZ domain or the substitution of its motif (LKV) with alanines resulted in impaired cell surface expression in cultured neurons and *in vivo* (15, 49). Residues 612–617 flanking the PDZ domain are also involved in hDAT retention and export from the ER (46). Similarly, the mutation of Lys^{590} and Asp^{600} impaired hDAT cell surface expression due to its retention in the ER, and the G585A substitution completely blocked hDAT export from the ER (50). Finally, the central motif FREKLAYAIA (residues 587–596) in hDAT has been suggested to be essential for the constitutive internalization of the transporter (22, 42–43). Thus, in all of these studies the potential involvement of the initial residues of DAT-CT in trafficking mechanisms was not described nor hypothesized.

The endocytosis of membrane proteins is typically mediated by signals present in their cytoplasmic domains, and these signals typically contain an essential tyrosine- or dileucine-based motif (51). Tyrosine-based motifs can be either NP*X*Y or Y*XX*Φ, where *X* is any amino acid, and Φ is a large, bulky hydrophobic residue. DAT contains no NP*X*Y sequence but does contain several Y*XX*Φ motifs. To our knowledge only one has been studied (^{335}YNKF in hDAT), but mutagenesis analyses ruled out any potential contribution of this motif to cell surface targeting or to PKC-mediated DAT internalization (52). Here, the YKF motif we identified to be involved in the binding of DAT to Ctr9 was positioned before a hydrophobic cysteine residue; thus, this sequence may be considered as a Y*XX*Φ motif. Because YKF mutation resulted in the cytoplasmic sequestration of DAT, this YKFC motif represents a strong candidate ER signal.

New Insight into the Structure of Ctr9—Ctr9 was first identified in the mouse as an SH2 domain binding phosphoprotein and was termed p150^{tsp} or TPR-containing SH2 binding phosphoprotein (24). This protein consists of 15 TPRDs arranged in tandem at the N terminus and a serine- and glutamic acid-rich C terminus that is essential for SH2 binding. Our results of three-dimensional modeling and sequence alignment between Ctr9 and crystallized TPRD-containing proteins revealed the

presence of three novel TPRDs in Ctr9, located between the N terminus and TPRD1, between TPRD9 and -10, and between TPRD14 and -15. Analysis of the primary Ctr9 sequence confirmed the presence of the TPR consensus. Indeed, the TPR motif is defined as a degenerate, 34-amino acid repeat displaying a largely conserved pattern of residue similarity or homology in terms of size, hydrophobicity, and spacing. In particular, eight residues appeared at a comparatively higher frequency of conservation to generate a consensus sequence at positions 4 (Trp/Leu/Phe), 7 (Leu/Ile/Met), 8 (Gly/Ala/Ser), 11 (Tyr/Leu/Phe), 20 (Ala/Ser/Glu), 24 (Phe/Tyr/Leu), 27 (Ala/Ser/Leu), and 32 (Pro/Lys/Glu) (53, 54). To date, almost all previously characterized TPRDs from several proteins, including Ctr9, contain four to seven of these conserved motifs. Here, the newly identified TPR domains of Ctr9 display five to six of them, strongly supporting that Ctr9 contains 18, not 15, TPRDs.

The Interaction between DAT and Ctr9 Modulates DAT Activity—Previously identified DAT-interacting proteins have been suggested to regulate DAT function by changing its subcellular distribution, trafficking, and/or functional properties. For instance, the interaction of DAT with PICK1 (PKC-interacting protein-1) leads to a redistribution of both proteins into clusters and, therefore, an enhancement of DAT activity due to an increased number of transporters at the plasma membrane (15). Similarly, α-synuclein and the D_{2S} receptor facilitate the recruitment of intracellular DAT to the plasma membrane, resulting in an augmentation of DA reuptake (14, 19). By contrast, Hic-5 reduces DAT activity and cell surface expression (16).

In this study we demonstrated that DAT-mediated DA uptake is increased in the presence of Ctr9. Analysis of the kinetic properties of DAT revealed an increase in V_{max} with no change in K_m. Therefore, we performed biotinylation experiments, which showed that the Ctr9-mediated enhancement of DAT activity reflects an increase in the number of transporters at the cell surface. We also confirmed, as previously reported (48), that both the immature (50 kDa) and fully mature (90 kDa) forms of DAT are localized to the plasma membrane. Interestingly, we observed that even though Ctr9 expression leads to an increased level of both forms of DAT at the plasma membrane, this up-regulation is more important for the fully mature form of DAT than for the immature form. These results suggest that Ctr9 alters the subcellular distribution of DAT and its trafficking from the ER and the Golgi, where DAT maturation occurs, to the plasma membrane.

New Insight into the Compartmental Localization of Ctr9—The Ctr9 protein was originally described to be predominantly or exclusively localized to the nucleus (24). In this report we first confirmed that Ctr9 is largely localized to the nucleus but is also clearly present in the cytoplasm and in some cell processes using two different tagged proteins (HA- and Myc-tagged Ctr9). We also demonstrated that the loss of the SH2 binding domain of Ctr9 led to the complete redistribution of Ctr9 to the cytoplasm. Our results were supported by sequence analysis using the pSPORTII server, which predicted a nuclear subcellular localization for the entire protein (91.3%) and a cytoplasmic distribution for Ctr9ΔSH2 (91.3%). We propose that Ctr9 translocation to the cytoplasm is dependent on interactions (or the loss of interactions) between the SH2 domain and nuclear proteins.

Studies of Ctr9 function in the nucleus showed that Ctr9 is a component of the Paf1 complex, which associates with RNA polymerase II (25, 55–57) and is involved in multiple transcription-related processes (for review, see Ref. 26). Other functions of Ctr9 have been suggested. In *Saccharomyces cerevisiae,* CDP1, a yeast homolog of Ctr9, is thought to play a role in regulating tubulin dynamics in the cell and may directly interact with microtubules or tubulin, resulting in improper chromosome segregation and nuclear division (58). Analysis of the *Saccharomyces pombe* homolog Tpr1 revealed that this protein might trigger potassium uptake via conventional transporters (59). However, none of these studies identified a non-nuclear Ctr9 protein binding partner or a function of Ctr9 outside the nucleus. The identification of a direct interaction of Ctr9 with DAT has thus ascribed a novel role to this protein.

Dual Roles of Ctr9 in the Nucleus and the Cytoplasm—One principal finding of our study was the identification of a role of Ctr9 outside the nucleus. In fact, two examples of such dual activity have been reported. The first example is DREAM, a Ca^{2+}-sensitive transcriptional repressor that is also known as KChiP-3, or K^+ channel-interacting protein 3. In the ER, DREAM/KChip-3 interacts with Kv4 channels to facilitate the appropriate trafficking and membrane expression of these potassium channels (60, 61). Similarly, it was shown that outside the nucleus, the transcription factor TFII-I acts as a negative regulator of agonist-induced calcium entry to suppress the cell surface accumulation of transient receptor potential channel-3 (TRPC3). In this model, TFII-I suppresses agonist-induced calcium entry by interfering with the protein-protein interaction between TRPC3 and phospholipase Cγ (62).

Based on yeast two-hybrid and GST pulldown experiments, we found that the physical interaction between Ctr9 and DAT is extremely robust. However, we do not know at present whether the V_{max} increase that we observed is a direct consequence of this interaction. For instance, it is possible that Ctr9 might facilitate DAT export from the ER by masking the putative YKFC motif of DAT, a potential consensus sequence for ER localization. This hypothesis is supported by (i) DAT sequestration in the cytoplasm after the mutation of the YKF motif and (ii) the preferential increase of the fully mature form of DAT at the plasma membrane after Ctr9 overexpression. This latter point suggests that transporter molecules further mature in the Golgi, implying that the transporters first exit the ER. Alternatively, the effect of Ctr9 on DAT may be a consequence of the Ctr9-induced displacement of other DAT-interacting proteins. For example, Ctr9 may interfere with the interaction between Hic-5 and DAT. Indeed, residues 571–580 of DAT, which interact with Hic-5, overlap with the YKF motif, which is required for the DAT-Ctr9 interaction. Because Hic-5 acts as a negative regulator of DAT function, the interaction of Ctr9 with DAT may inhibit the binding of Hic-5 to the transporter, thereby leading to increased DAT activity.

Interestingly, our findings indicate a possible relationship between transcription and neurotransmission via the trafficking of Ctr9 between the nuclear and plasma membrane compartments. Whether Ctr9 displays a Janus face-like activity in

which each compartmental role is fully independent or performs a shuttle function between the nucleus and the cytoplasm remains an intriguing question for future experiments.

Author Contributions—The studies were conceived and designed by B. G. and S. D. G. Experiments were performed by S. D. G. with P. S., A. M. E., F. L., and C. B.-V. L. D performed the Y2H screen, and N. P. performed the structural analysis. The paper was written by B. G. and S. D. G. and was edited by the other authors.

Acknowledgments—We thank Dr. Philippe Vernier (CNRS, Gif-sur-Yvette, France) for involvement and discussions in the early stage of this project and Dr. Stephen Desiderio (Johns Hopkins University) for the gift of a Ctr9 plasmid. We benefited from excellent technical support from Gaël Grannec (mouse breeding), Annie Munier (Sercice Imagerie Cellulaire et Cytométrie en Flux, IBPS, Université Pierre et Marie Curie, Paris, France), and Biliana Todorova (GST pulldown setup).

References

1. Nieoullon, A. (2002) Dopamine and the regulation of cognition and attention. *Prog. Neurobiol.* **67,** 53–83
2. Fon, E. A., and Edwards, R. H. (2001) Molecular mechanisms of neurotransmitter release. *Muscle Nerve* **24,** 581–601
3. Lin, Z., Canales, J. J., Björgvinsson, T., Thomsen, M., Qu, H., Liu, Q. R., Torres, G. E., and Caine, S. B. (2011) Monoamine transporters: vulnerable and vital doorkeepers. *Prog. Mol. Biol. Transl. Sci.* **98,** 1–46
4. Giros, B., and Caron, M. G. (1993) Molecular characterization of the dopamine transporter. *Trends Pharmacol. Sci.* **14,** 43–49
5. Giros, B., Jaber, M., Jones, S. R., Wightman, R. M., and Caron, M. G. (1996) Hyperlocomotion and indifference to cocaine and amphetamine in mice lacking the dopamine transporter. *Nature* **379,** 606–612
6. Jones, S. R., Gainetdinov, R. R., Jaber, M., Giros, B., Wightman, R. M., and Caron, M. G. (1998) Profound neuronal plasticity in response to inactivation of the dopamine transporter. *Proc. Natl. Acad. Sci. U.S.A.* **95,** 4029–4034
7. Gainetdinov, R. R., Wetsel, W. C., Jones, S. R., Levin, E. D., Jaber, M., and Caron, M. G. (1999) Role of serotonin in the paradoxical calming effect of psychostimulants on hyperactivity. *Science* **283,** 397–401
8. Mortensen, O. V., and Amara, S. G. (2003) Dynamic regulation of the dopamine transporter. *Eur. J. Pharmacol.* **479,** 159–170
9. Pristupa, Z. B., McConkey, F., Liu, F., Man, H. Y., Lee, F. J., Wang, Y. T., and Niznik, H. B. (1998) Protein kinase-mediated bidirectional trafficking and functional regulation of the human dopamine transporter. *Synapse* **30,** 79–87
10. Daniels, G. M., and Amara, S. G. (1999) Regulated trafficking of the human dopamine transporter. Clathrin-mediated internalization and lysosomal degradation in response to phorbol esters. *J. Biol. Chem.* **274,** 35794–35801
11. Melikian, H. E., and Buckley, K. M. (1999) Membrane trafficking regulates the activity of the human dopamine transporter. *J. Neurosci.* **19,** 7699–7710
12. Chang, M. Y., Lee, S. H., Kim, J. H., Lee, K. H., Kim, Y. S., Son, H., and Lee, Y. S. (2001) Protein kinase C-mediated functional regulation of dopamine transporter is not achieved by direct phosphorylation of the dopamine transporter protein. *J. Neurochem.* **77,** 754–761
13. Granas, C., Ferrer, J., Loland, C. J., Javitch, J. A., and Gether, U. (2003) N-terminal truncation of the dopamine transporter abolishes phorbol ester- and substance P receptor-stimulated phosphorylation without impairing transporter internalization. *J. Biol. Chem.* **278,** 4990–5000
14. Lee, F. J., Liu, F., Pristupa, Z. B., and Niznik, H. B. (2001) Direct binding and functional coupling of α-synuclein to the dopamine transporters accelerate dopamine-induced apoptosis. *FASEB J.* **15,** 916–926
15. Torres, G. E., Yao, W. D., Mohn, A. R., Quan, H., Kim, K. M., Levey, A. I., Staudinger, J., and Caron, M. G. (2001) Functional interaction between monoamine plasma membrane transporters and the synaptic PDZ domain-containing protein PICK1. *Neuron* **30,** 121–134
16. Carneiro, A. M., Ingram, S. L., Beaulieu, J. M., Sweeney, A., Amara, S. G., Thomas, S. M., Caron, M. G., and Torres, G. E. (2002) The multiple LIM domain-containing adaptor protein Hic-5 synaptically colocalizes and interacts with the dopamine transporter. *J. Neurosci.* **22,** 7045–7054
17. Lee, K. H., Kim, M. Y., Kim, D. H., and Lee, Y. S. (2004) Syntaxin 1A and receptor for activated C kinase interact with the N-terminal region of human dopamine transporter. *Neurochem. Res.* **29,** 1405–1409
18. Moszczynska, A., Saleh, J., Zhang, H., Vukusic, B., Lee, F. J., and Liu, F. (2007) Parkin disrupts the α-synuclein/dopamine transporter interaction: consequences toward dopamine-induced toxicity. *J. Mol. Neurosci.* **32,** 217–227
19. Lee, F. J., Pei, L., Moszczynska, A., Vukusic, B., Fletcher, P. J., and Liu, F. (2007) Dopamine transporter cell surface localization facilitated by a direct interaction with the dopamine D2 receptor. *EMBO J.* **26,** 2127–2136
20. Castro-Hernández, J., Afonso-Oramas, D., Cruz-Muros, I., Salas-Hernández, J., Barroso-Chinea, P., Moratalla, R., Millan, M. J., and González-Hernández, T. (2015) Prolonged treatment with pramipexole promotes physical interaction of striatal dopamine D3 autoreceptors with dopamine transporters to reduce dopamine uptake. *Neurobiol. Dis.* **74,** 325–335
21. Egaña, L. A., Cuevas, R. A., Baust, T. B., Parra, L. A., Leak, R. K., Hochendoner, S., Peña, K., Quiroz, M., Hong, W. C., Dorostkar, M. M., Janz, R., Sitte, H. H., and Torres, G. E. (2009) Physical and functional interaction between the dopamine transporter and the synaptic vesicle protein synaptogyrin-3. *J. Neurosci.* **29,** 4592–4604
22. Navaroli, D. M., Stevens, Z. H., Uzelac, Z., Gabriel, L., King, M. J., Lifshitz, L. M., Sitte, H. H., and Melikian, H. E. (2011) The plasma membrane-associated GTPase Rin interacts with the dopamine transporter and is required for protein kinase C-regulated dopamine transporter trafficking. *J. Neurosci.* **31,** 13758–13770
23. Garcia-Olivares, J., Torres-Salazar, D., Owens, W. A., Baust, T., Siderovski, D. P., Amara, S. G., Zhu, J., Daws, L. C., and Torres, G. E. (2013) Inhibition of dopamine transporter activity by G protein $\beta\gamma$ subunits. *PLoS ONE* **8,** e59788
24. Malek, S. N., Yang, C. H., Earnshaw, W. C., Kozak, C. A., and Desiderio, S. (1996) p150TSP, a conserved nuclear phosphoprotein that contains multiple tetratricopeptide repeats and binds specifically to SH2 domains. *J. Biol. Chem.* **271,** 6952–6962
25. Youn, M. Y., Yoo, H. S., Kim, M. J., Hwang, S. Y., Choi, Y., Desiderio, S. V., and Yoo, J. Y. (2007) hCTR9, a component of Paf1 complex, participates in the transcription of interleukin 6-responsive genes through regulation of STAT3-DNA interactions. *J. Biol. Chem.* **282,** 34727–34734
26. Jaehning, J. A. (2010) The Paf1 complex: Platform or player in RNA polymerase II transcription? *Biochim. Biophys. Acta* **1799,** 379–388
27. Vinatier, J., Herzog, E., Plamont, M. A., Wojcik, S. M., Schmidt, A., Brose, N., Daviet, L., El Mestikawy, S., and Giros, B. (2006) Interaction between the vesicular glutamate transporter type 1 and endophilin A1, a protein essential for endocytosis. *J. Neurochem.* **97,** 1111–1125
28. Thompson, J. D., Higgins, D. G., and Gibson, T. J. (1994) ClustalW: improving the sensitivity of progressive multiple sequence alignment through sequence weighting, position-specific gap penalties and weight matrix choice. *Nucleic Acids Res.* **22,** 4673–4680
29. Eddy, S. R. (2004) Where did the BLOSUM62 alignment score matrix come from? *Nat. Biotechnol.* **22,** 1035–1036
30. Krogh, A., Larsson, B., von Heijne, G., and Sonnhammer, E. L. (2001) Predicting transmembrane protein topology with a hidden Markov model: application to complete genomes. *J. Mol. Biol.* **305,** 567–580
31. Tusnády, G. E., and Simon, I. (2001) The HMMTOP transmembrane topology prediction server. *Bioinformatics* **17,** 849–850
32. Malherbe, P., Kratochwil, N., Knoflach, F., Zenner, M. T., Kew, J. N., Kratzeisen, C., Maerki, H. P., Adam, G., and Mutel, V. (2003) Mutational analysis and molecular modeling of the allosteric binding site of a novel, selective, noncompetitive antagonist of the metabotropic glutamate 1 receptor. *J. Biol. Chem.* **278,** 8340–8347
33. Fiser, A., and Sali, A. (2003) Modeller: generation and refinement of homology-based protein structure models. *Methods Enzymol.* **374,** 461–491
34. Bowie, J. U., Lüthy, R., and Eisenberg, D. (1991) A method to identify

protein sequences that fold into a known three-dimensional structure. *Science* **253,** 164–170
35. Bessis, A. S., Bertrand, H. O., Galvez, T., De Colle, C., Pin, J. P., and Acher, F. (2000) Three-dimensional model of the extracellular domain of the type 4a metabotropic glutamate receptor: new insights into the activation process. *Protein Sci.* **9,** 2200–2209
36. Ramachandran, G. N., Ramakrishnan, C., and Sasisekharan, V. (1963) Stereochemistry of polypeptide chain configurations. *J. Mol. Biol.* **7,** 95–99
37. Li, L., Chen, R., and Weng, Z. (2003) RDOCK: refinement of rigid-body protein docking predictions. *Proteins* **53,** 693–707
38. Masson, J., Riad, M., Chaudhry, F., Darmon, M., Aïdouni, Z., Conrath, M., Giros, B., Hamon, M., Storm-Mathisen, J., Descarries, L., and El Mestikawy, S. (1999) Unexpected localization of the Na^+/Cl^--dependent-like orphan transporter, Rxt1, on synaptic vesicles in the rat central nervous system. *Eur. J. Neurosci.* **11,** 1349–1361
39. De Gois, S., Schäfer, M. K., Defamie, N., Chen, C., Ricci, A., Weihe, E., Varoqui, H., and Erickson, J. D. (2005) Homeostatic scaling of vesicular glutamate and GABA transporter expression in rat neocortical circuits. *J. Neurosci.* **25,** 7121–7133
40. Giros, B., el Mestikawy, S., Godinot, N., Zheng, K., Han, H., Yang-Feng, T., and Caron, M. G. (1992) Cloning, pharmacological characterization, and chromosome assignment of the human dopamine transporter. *Mol. Pharmacol.* **42,** 383–390
41. Giros, B., el Mestikawy, S., Bertrand, L., and Caron, M. G. (1991) Cloning and functional characterization of a cocaine-sensitive dopamine transporter. *FEBS Lett.* **295,** 149–154
42. Holton, K. L., Loder, M. K., and Melikian, H. E. (2005) Nonclassical, distinct endocytic signals dictate constitutive and PKC-regulated neurotransmitter transporter internalization. *Nat. Neurosci.* **8,** 881–888
43. Boudanova, E., Navaroli, D. M., Stevens, Z., and Melikian, H. E. (2008) Dopamine transporter endocytic determinants: carboxy terminal residues critical for basal and PKC-stimulated internalization. *Mol. Cell. Neurosci.* **39,** 211–217
44. Torres, G. E., Sweeney, A. L., Beaulieu, J. M., Shashidharan, P., and Caron, M. G. (2004) Effect of torsinA on membrane proteins reveals a loss of function and a dominant-negative phenotype of the dystonia-associated deltaE-torsinA mutant. *Proc. Natl. Acad. Sci. U.S.A.* **101,** 15650–15655
45. Hervé, F., Ghinea, N., and Scherrmann, J. M. (2008) CNS delivery via adsorptive transcytosis. *Aaps J.* **10,** 455–472
46. Bjerggaard, C., Fog, J. U., Hastrup, H., Madsen, K., Loland, C. J., Javitch, J. A., and Gether, U. (2004) Surface targeting of the dopamine transporter involves discrete epitopes in the distal C terminus but does not require canonical PDZ domain interactions. *J. Neurosci.* **24,** 7024–7036
47. Li, L. B., Chen, N., Ramamoorthy, S., Chi, L., Cui, X. N., Wang, L. C., and Reith, M. E. (2004) The role of *N*-glycosylation in function and surface trafficking of the human dopamine transporter. *J. Biol. Chem.* **279,** 21012–21020
48. Torres, G. E., Carneiro, A., Seamans, K., Fiorentini, C., Sweeney, A., Yao, W. D., and Caron, M. G. (2003) Oligomerization and trafficking of the human dopamine transporter. Mutational analysis identifies critical domains important for the functional expression of the transporter. *J. Biol. Chem.* **278,** 2731–2739
49. Rickhag, M., Hansen, F. H., Sørensen, G., Strandfelt, K. N., Andresen, B., Gotfryd, K., Madsen, K. L., Vestergaard-Klewe, I., Ammendrup-Johnsen, I., Eriksen, J., Newman, A. H., Füchtbauer, E. M., Gomeza, J., Woldbye, D. P., Wörtwein, G., and Gether, U. (2013) A C-terminal PDZ domain-binding sequence is required for striatal distribution of the dopamine transporter. *Nat. Commun.* **4,** 1580
50. Miranda, M., Sorkina, T., Grammatopoulos, T. N., Zawada, W. M., and Sorkin, A. (2004) Multiple molecular determinants in the carboxyl terminus regulate dopamine transporter export from endoplasmic reticulum. *J. Biol. Chem.* **279,** 30760–30770
51. Bonifacino, J. S., and Traub, L. M. (2003) Signals for sorting of transmembrane proteins to endosomes and lysosomes. *Annu. Rev. Biochem.* **72,** 395–447
52. Loland, C. J., Norregaard, L., Litman, T., and Gether, U. (2002) Generation of an activating Zn^{2+} switch in the dopamine transporter: mutation of an intracellular tyrosine constitutively alters the conformational equilibrium of the transport cycle. *Proc. Natl. Acad. Sci. U.S.A.* **99,** 1683–1688
53. Sikorski, R. S., Boguski, M. S., Goebl, M., and Hieter, P. (1990) A repeating amino acid motif in CDC23 defines a family of proteins and a new relationship among genes required for mitosis and RNA synthesis. *Cell* **60,** 307–317
54. Blatch, G. L., and Lässle, M. (1999) The tetratricopeptide repeat: a structural motif mediating protein-protein interactions. *Bioessays* **21,** 932–939
55. Koch, C., Wollmann, P., Dahl, M., and Lottspeich, F. (1999) A role for Ctr9p and Paf1p in the regulation G_1 cyclin expression in yeast. *Nucleic Acids Res.* **27,** 2126–2134
56. Mueller, C. L., and Jaehning, J. A. (2002) Ctr9, Rtf1, and Leo1 are components of the Paf1/RNA polymerase II complex. *Mol. Cell. Biol.* **22,** 1971–1980
57. Marton, H. A., and Desiderio, S. (2008) The Paf1 complex promotes displacement of histones upon rapid induction of transcription by RNA polymerase II. *BMC Mol. Biol.* **9,** 4
58. Foreman, P. K., and Davis, R. W. (1996) CDP1, a novel *Saccharomyces cerevisiae* gene required for proper nuclear division and chromosome segregation. *Genetics* **144,** 1387–1397
59. Lichtenberg, H., Heyer, M., and Höfer, M. (1999) pr1, a Schizosaccharomyces pombe protein involved in potassium transport. *FEBS letters* **457,** 363–368
60. An, W. F., Bowlby, M. R., Betty, M., Cao, J., Ling, H. P., Mendoza, G., Hinson, J. W., Mattsson, K. I., Strassle, B. W., Trimmer, J. S., and Rhodes, K. J. (2000) Modulation of A-type potassium channels by a family of calcium sensors. *Nature* **403,** 553–556
61. Shibata, R., Misonou, H., Campomanes, C. R., Anderson, A. E., Schrader, L. A., Doliveira, L. C., Carroll, K. I., Sweatt, J. D., Rhodes, K. J., and Trimmer, J. S. (2003) A fundamental role for KChIPs in determining the molecular properties and trafficking of Kv4.2 potassium channels. *J. Biol. Chem.* **278,** 36445–36454
62. Caraveo, G., van Rossum, D. B., Patterson, R. L., Snyder, S. H., and Desiderio, S. (2006) Action of TFII-I outside the nucleus as an inhibitor of agonist-induced calcium entry. *Science* **314,** 122–125